Front. Struct. Civ. Eng. 2023, 17(4): 522–532
https://doi.org/10.1007/s11709-023-0930-9

RESEARCH ARTICLE

Effect of cutterhead configuration on tunnel face stability during shield machine maintenance outages

Yinzun YANG[a,b], Dajun YUAN[a,b], Dalong JIN[a,b*]

[a] *Key Laboratory of the Ministry of Education for Urban Underground Engineering, Beijing Jiaotong University, Beijing 100044, China*

[b] *School of Civil Engineering, Beijing Jiaotong University, Beijing 100044, China*

[*] *Corresponding author. E-mail: jindalong@163.com*

ABSTRACT Owing to long-distance advancement or obstacles, shield tunneling machines are typically shut down for maintenance. Engineering safety during maintenance outages is determined by the stability of the tunnel face. Pressure maintenance openings are typically used under complicated hydrogeological conditions. The tunnel face is supported by a medium at the bottom of the excavation chamber and compressed air at the top. Owing to the high risk of face failure, the necessity of support pressure when cutterhead support is implemented and a method for determining the value of compressed air pressure using different support ratios must to be determined. In this study, a non-fully chamber supported rotational failure model considering cutterhead support is developed based on the upper-bound theorem of limit analysis. Numerical simulation is conducted to verify the accuracy of the proposed model. The results indicate that appropriately increasing the specific gravity of the supporting medium can reduce the risk of collapse. The required compressed air pressure increases significantly as the support ratio decreases. Disregarding the supporting effect of the cutterhead will result in a tunnel face with underestimated stability. To satisfy the requirement of chamber openings at atmospheric pressure, the stratum reinforcement strength and range at the shield end are provided based on different cutterhead aperture ratios.

KEYWORDS tunnel face stability, cutterhead configuration, aperture ratio, pressure gradient, support ratio

1 Introduction

With the rapid increase in underground engineering, construction in China has resulted in an increase in shield tunneling. Shield construction presents many technical problems, such as tunnel face failure [1–4], tool wear [5–8], and segment leakage [9–11]. The increase in long-advance and super large-diameter shield projects has resulted in a higher occurrence of shield tunneling machines being shut down because of obstacles or for machine maintenance. Shield machine maintenance during shutdown is typically performed using an atmospheric pressure opening or a pressure maintenance opening [12]. The atmospheric pressure opening is only suitable for a stratum with a high self-steady ability. In an environment with complicated hydrogeological conditions, a large cover depth, or a high hydraulic pressure, only pressure maintenance openings can be adopted. The chamber opening is used to achieve a safe and stable maintenance environment. Therefore, the excavation chamber opening is governed by the stability of the tunnel face.

In shield construction, the external pressure of the soil and water is balanced by the support pressure from the soil muck or bentonite slurry in the excavation chamber. The soil propagates into the excavation chamber rapidly when the support pressure is insufficient, resulting in active ground instability accidents [13–15]. In recent years, the failure mechanism of tunnel faces has been investigated extensively via theoretical analysis [16–19], model tests [20–23], and numerical simulations [24,25].

Mollon et al. [26] proposed a three-dimensional (3D)

Article history: Received Sep 13, 2022; Accepted Oct 31, 2022

rotational failure model, and both the upper and lower solutions of the critical support pressures were provided. Perazzelli [27] derived a closed-form solution for the lower solution of the limit support pressure under seepage flow conditions. Pan and Dias [28] investigated the effect of anisotropic permeability on the limit solution of critical support pressure using a kinematic method and the FLAC3D software. Ji et al. [29] investigated the effects of tunnel diameter and cover depth on support pressure; the 3D arch effect was considered as well in that study. Kirsch [30] investigated the critical support pressure of a tunnel face in dry sandy ground via model tests. The results indicated that the initial density of the ground significantly affected the development of the collapse mechanism. Chen et al. [31] discussed the evolution process of a soil arch by performing model tests based on different soil covers. Qarmout et al. [32] proposed a numerical method to obtain the lower limit support pressure in dry frictional soil using the kinematic element method.

Owing to the space requirement of maintenance workers, cutters are typically inspected and changed under a non-fully supported mode [33], which can significantly reduce the face stability and easily cause ground collapse. In practical engineering, the top external pressure at the tunnel face is typically balanced with the compressed air pressure by reducing the fluid level of the muck or slurry in the chamber [34,35]. However, all previous studies focused on the analysis of face stability for cases involving uniformly and fully distributed support pressure in the excavation chamber, which can result in a tunnel face with overestimated stability. Additionally, the effect of the cutterhead is rarely considered when the shield machine is shut down. Most relevant previous studies are based on numerical simulations and do not involve theoretical calculations [36,37].

The current study investigates the face stability of shield tunneling machines shut down for pressure maintenance based on the kinematic approach of limit analysis. A non-fully chamber support model considering the cutterhead configuration is developed to evaluate the stability of the tunnel face based on the rotational failure mechanism proposed by Mollon et al. [26]. To validate the proposed mechanism, the limit support pressure is compared with numerical simulation results. The effects of the support ratio, pressure gradient, tunnel diameter, and aperture ratio are discussed. In addition, a reinforcement strength value and a limit reinforcement range of the stratum are proposed that can maintain the stability of the tunnel face when the shield tunneling machine is shut down.

2 3D rotational failure model

2.1 Support mode analysis considering cutterhead support

Based on the pressure distributions in the excavation chamber, Fig. 1 illustrates the chamber opening can be classified into two modes. a) The chamber opening at atmospheric pressure, where the excavation chamber is completely emptied. In this mode, the tunnel face is merely supported by the cutterhead. This model is only applicable to strata with good stability. b) The pressure maintenance chamber opening, where a certain height of the supporting medium is retained at the bottom of the excavation chamber. The external earth-water pressure at the top is balanced by the compressed air pressure [38–40]. This model is more suitable for unsatisfactory and water-rich stratum geological conditions. In the cutter changing period or for certain tunneling projects in a complex stratum, the tunnel face is supported entirely by compressed air pressure. However, controlling the accuracy of the compressed-air pressure adjustment is difficult. Moreover, the safety of maintenance workers may be jeopardized.

The bottom section of the tunnel face, supported by the

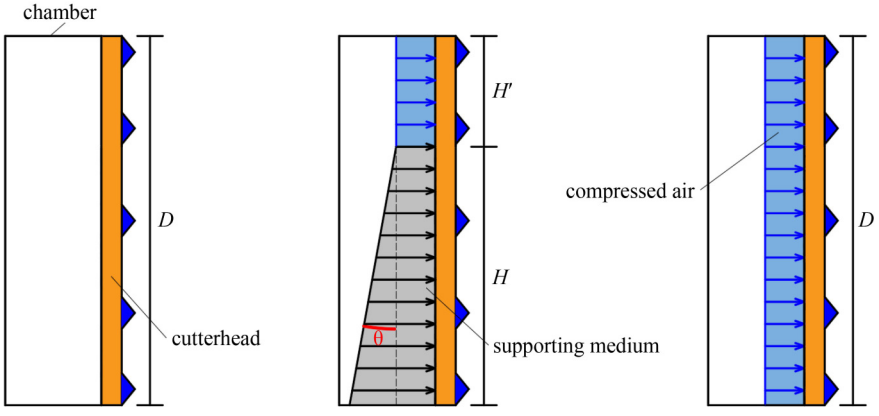

Fig. 1 Chamber opening modes: (a) chamber opening at atmospheric pressure; (b) pressure maintenance chamber opening. Notes: orange region: cutterhead; gray region: supporting medium pressure; blue region: compressed air pressure.

supporting medium, is known as the support face, whereas the upper section is a free face. The cover depth is denoted by C; the diameter of the shield tunnel, D; and the height of the support face, H. The support ratio n is defined as H/D, and σ_s is the limit support pressure of the supporting medium acting on the support face. The support pressure is distributed in trapezoidal form because of the soil gravity in the excavation chamber. As shown in Fig. 2, the gradient of the support pressure is denoted as k, which can be expressed as $k = \tan\theta$. The support pressure is uniformly distributed at $\theta = 0°$, and σ_A is the limit support pressure of compressed air supported on a free face. The cutterhead configuration is described by the aperture ratio μ [41]. In this study, the overall tunnel structure is considered safe, i.e., the cutterhead cannot propagate backward. Hence, only face stability problems are discussed herein.

2.2 Solution of critical support pressure

The limit support pressure calculation method used in this study is based on the theoretical rotational failure method proposed by Mollon et al. [26]. Its rationality has been verified based on numerous model test results for the active failure mechanism [30,42]. As shown in Fig. 3, a spatial discretization technique was used to model the rotational failure mechanism. The main purpose of modeling the 3D collapse mechanism is to generate a set of points that represent the contour in a previous plane. All the planes intersect at the origin of the polar coordinates, and the normal lines are parallel to the velocity field. The contour of the tunnel face is discretized by several points, and the moving block is discretized by several radial planes that coincide at point O. E is the center point of tunnel face. The boundary of the failure mechanism is determined only by two parameters, β_E and R_E/D, where β_E is the angle between OE and XY plane, R_E is the length. A and B are the intersection points of the spirochete and inverted arch with the central axis. In this study, the spirochete rotates around the central axis OX at a uniform angular velocity ω when global failure occurs. The velocity of each point in the spirochete mechanism is equal to the product of ω and the vertical distance from the point to OX. The tunnel face is discretized by m groups of points symmetric to the longitudinal axis OY.

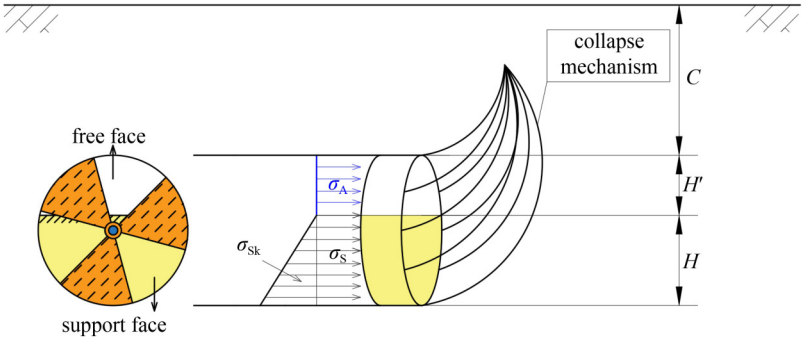

Fig. 2 Schematic diagram of the non-fully supported mode (σ_S: uniform support pressure, σ_{Sk}: gradient support pressure, σ_A: compressed air support pressure).

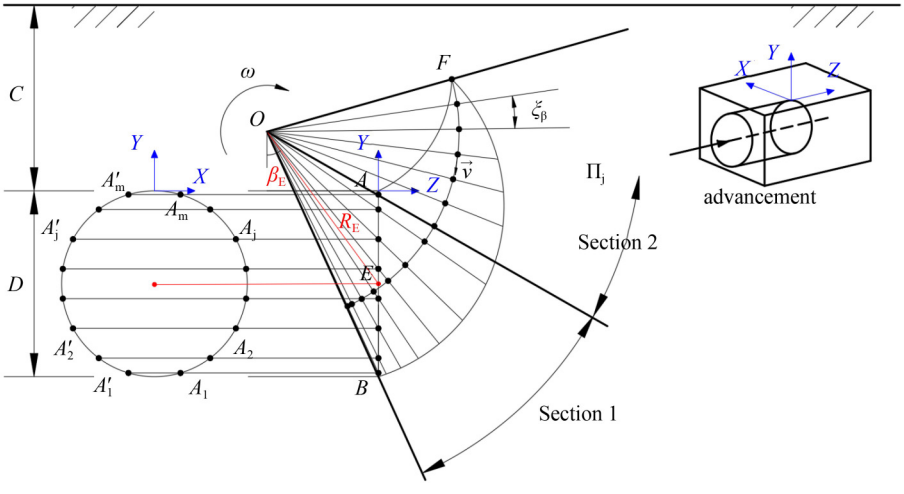

Fig. 3 Discretization technique for the collapse mechanism of tunnel face.

As shown in Fig. 3, the spirochete is composed of two sections. Both sections are discretized by several radial planes separated by ξ_β. In theory, the calculation accuracy is positively associated with ξ_β and m. However, the calculation time also increases as the accuracy increases. In this study, m and ξ_β were set as 100 and 1.0°, respectively.

In the upper-bound theorem of limit analysis, the ultimate state of active failure that occurs on the tunnel face is the work rate of the external force, which is equal to the internal energy dissipation. In this study, the rate of external face W_E includes the effective gravity of soil W_γ, support pressure $W_{\sigma T}$, and the uniform surcharge acting on the ground surface W_G when the failure mechanism outcrops. In this study, $W_{\sigma T}$ comprises three components: the work rate of the support force acting on the support face $W_{\sigma S}$, the compressed air support force acting on the free face $W_{\sigma A}$, and the static earth pressure from the cutterhead $W_{\sigma C}$. The distribution of σ_S, σ_A, σ_C is shown in Fig. 4(a). Based on the rotational collapse mechanism like Fig. 4(b) [26], the work rate of different external forces are presented next.

The work rate of the support force of the supporting medium is expressed as follows:

$$\begin{aligned} W_{\sigma S} &= \iint_S (\vec{\sigma}_S + \vec{\sigma}_{Sk}) \cdot \vec{v} \mathrm{d}\Sigma \\ &= -\omega \cdot \mu \cdot \left[k \cdot D \cdot \sum_{j=1}^{nm} (n - j/m) + \sigma_S \right] \\ &\quad \cdot \sum_{j=1}^{nm} (S_j \cdot R_j \cdot \cos\beta_j), \end{aligned} \tag{1}$$

where σ_S denotes the uniform support pressure acting on the support face and σ_{Sk} is the gradient support pressure applied to the support face. The height of the support face is adjusted by nD. Similarly, the support area is changed by adjusting the summation of the upper bound, nm. In this study, the specific gravity of the soil or slurry is adjusted by the gradient k, R_j and β_j are the polar coordinates of the points on the support face, S_j represents the area of the element at the discretized face, ω is the angular velocity of the failure mechanism, and μ is the aperture ratio of the cutterhead.

The work rate of compressed air support force acting on the free face is expressed as follows:

$$W_{\sigma A} = \iint_S \overrightarrow{\sigma_A} \cdot \overrightarrow{v} \mathrm{d}\Sigma = -\omega \cdot \mu \cdot \sigma_A \cdot \sum_{j=nm+1}^{m-1} (S_j \cdot R_j \cdot \cos\beta_j), \tag{2}$$

where σ_A denotes the compressed air pressure acting on the free face. For the non-fully supported mode with compressed air pressure, σ_A is uniformly distributed and equal to σ_S [34]. In the non-fully supported mode analysis, $\sigma_A = 0$.

The work rate of the cutterhead support force acting on the tunnel face is expressed as follows:

$$W_C = \iint_S \overrightarrow{\sigma_C} \cdot \vec{v} \mathrm{d}\Sigma = -\omega \cdot k_0 \cdot \gamma \cdot (1-\mu) \cdot \sum_{j=1}^{m-1} S_j \cdot R_j \cdot H_j \cdot \cos\beta_j, \tag{3}$$

where σ_C denotes the support pressure of the cutterhead acting on the tunnel face. In practice, a shield machine cannot be retreated owing to the jacking force from the thrust cylinders. Hence, suppose that the support pressure of the cutterhead is equal to the static earth pressure for each trip; k_0 is the lateral pressure coefficient, whose value is set as 0.35 to indicate the empirical value of tunneling in sandy soil [43]; γ is the unit weight of the stratum; and H_j is the cover depth of the element on the discretized face.

The work rate of possible uniform surcharge acting on the ground surface can be expressed as

$$W_G = \iint_S \overrightarrow{\sigma_G} \cdot \overrightarrow{v} \mathrm{d}\Sigma = \omega \cdot \sigma_G \cdot \sum_l (S_l \cdot R_l \cdot \sin\beta_l), \tag{4}$$

where σ_G denotes the ground surface surcharge, R_l and β_l are the polar coordinates of the points on the possible outcropping surface, and S_l represents the area of an element on the outcropping surface. In this study, only the active failure problem is considered, whereas W_G is not.

The work rate of effective gravity is expressed as

$$\begin{aligned} W_\gamma &= \iiint_V \vec{\gamma} \cdot \vec{v} \mathrm{d}V \\ &= \omega \cdot \gamma \cdot \sum_{i,j} (R_{i,j} \cdot V_{i,j} \cdot \sin\beta_{i,j} + R'_{i,j} \cdot V'_{i,j} \cdot \sin\beta'_{i,j}), \end{aligned} \tag{5}$$

where $R_{i,j}$ and $\beta_{i,j}$ (and the corresponding $R'_{i,j}$ and $\beta'_{i,j}$) are the polar coordinates of the surface center of gravity of discrete micro-tetrahedral elements in the collapse mechanism, and $V_{i,j}$ (and the corresponding $V'_{i,j}$) is the micro-tetrahedral unit volume.

In this study, internal energy dissipation only includes the soil sliding resistance W_S.

$$W_S = \iint_S c \cdot v \cdot \cos\varphi \cdot \mathrm{d}S = \omega \cdot c \cdot \cos\varphi \cdot \sum_{i,j} (S_{i,j} \cdot R_{i,j} + S'_{i,j} \cdot R'_{i,j}), \tag{6}$$

where c is the cohesion of stratum soil; φ is the angle of the internal friction; and $S_{i,j}$ and $S'_{i,j}$ are the areas of triangular faces $P_{i,j}P_{i+1,j}P_{i,j+1}$ and $P_{i+1,j}P_{i,j+1}P_{i+1,j+1}$, respectively.

Based on the upper-bound theorem of limit analysis, the upper-bound value of the limit support pressure can be derived as follows [44]:

$$\sigma_S = \gamma D N_\gamma - cN_S + \sigma_G N_G - kD\mu N_k - k_0\gamma(1-\mu)N_C. \tag{7}$$

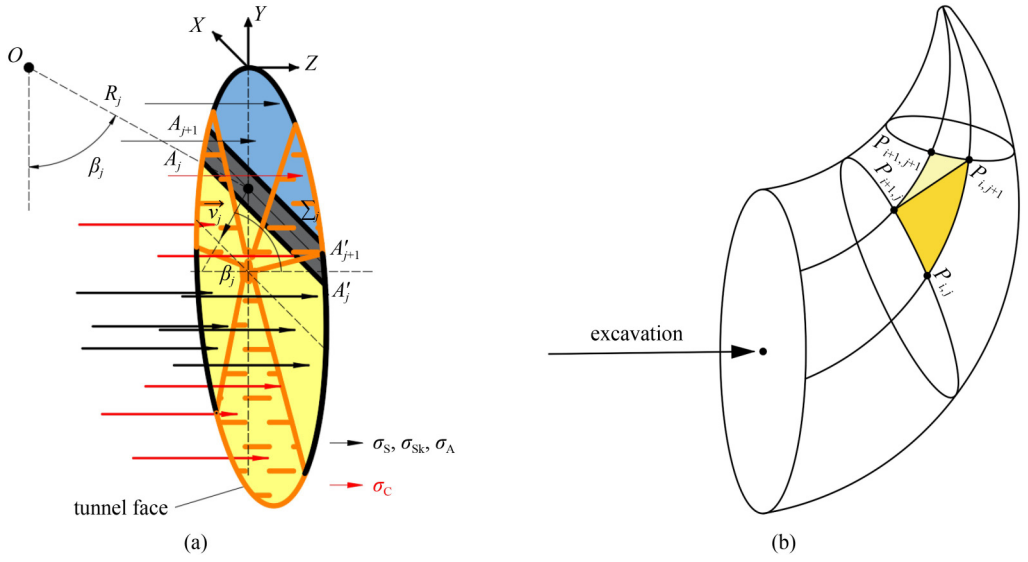

Fig. 4 (a) Computation of work rates of tunnel face (v_j represents the velocity of the discretized element on tunnel face); (b) schematic illustration of rotational failure mechanism.

The limit collapse support pressure can be obtained by maximizing σ_S in Eq. (7). In the equation, N_γ, N_S, N_G, N_k, and N_C are dimensionless coefficients associated with the soil weight, cohesion, surface load, support modes, and cutterhead configuration impact factor, respectively. Their formulas are shown as follows:

$$N_\gamma = \frac{\sum_{i,j}(R_{i,j}\cdot V_{i,j}\cdot \sin\beta_{i,j} + R'_{i,j}\cdot V'_{i,j}\cdot \sin\beta'_{i,j})}{D\cdot \sum_j (S_j\cdot R_j\cdot \cos\beta_j)}, \quad (8)$$

$$N_S = \frac{\cos\varphi\cdot \sum_{i,j}(S_{i,j}\cdot R_{i,j} + S'_{i,j}\cdot R'_{i,j})}{\sum_j (S_j\cdot R_j\cdot \cos\beta_j)}, \quad (9)$$

$$N_G = \frac{\sum_l (S_l\cdot R_l\cdot \sin\beta_l)}{\sum_j (S_j\cdot R_j\cdot \cos\beta_j)}, \quad (10)$$

$$N_k = \frac{\sum_{j=1}^{nm}[(n-j/m)\cdot S_j\cdot R_j\cdot \cos\beta_j]}{\sum_j (S_j\cdot R_j\cdot \cos\beta_j)}, \quad (11)$$

$$N_C = \frac{\sum_{j=1}^{m-1}[S_j\cdot R_j\cdot H_j\cdot \cos\beta_j]}{\sum_j (S_j\cdot R_j\cdot \cos\beta_j)}. \quad (12)$$

3 Comparisons

3.1 FLAC3D modeling

To verify the accuracy of the proposed theory, a tunnel face without cutterhead support (μ = 100%), a tunnel face supported by a spoke cutterhead (μ = 51.52%), and a spoke-panel cutterhead (μ = 26.61%) were simulated using FLAC3D. As shown in Fig. 5, the size of the 3D model was 40 m (length) × 50 m (width) × 30 m (height). The width was set to five times the tunnel diameter D. Both cover depths, C and D, were set to 10 m. The thicknesses of the cutterhead and shell were set as 0.3 m. To accurately describe the stratum slip trend, the mesh density was increased within 5 m in front of the tunnel face [45]. The top of the model was constrained by a free boundary, the surroundings were constrained by a normal displacement, and the bottom was a fixed boundary. The soil properties were described using the Mohr–Coulomb constitutive model. A linear elastic model was adopted to simulate the cutterhead and shell of the shield machine. The detailed parameters are listed in Table 1. On the tunnel face, only a uniform support pressure was applied to the free face. Uniform and gradient support pressures were applied to the support face. Static earth pressure in the form of a gradient was applied to the cutterhead region.

3.2 Determination of face failure

An improved dichotomy method was used in this study to determine the limit support pressure via numerical simulation [16]. This method comprises three basic steps: 1) the cohesion of the stratum is set to an extremely high value, which transforms the soil into an elastic material; 2) the internal stress is manually set to twice the initial

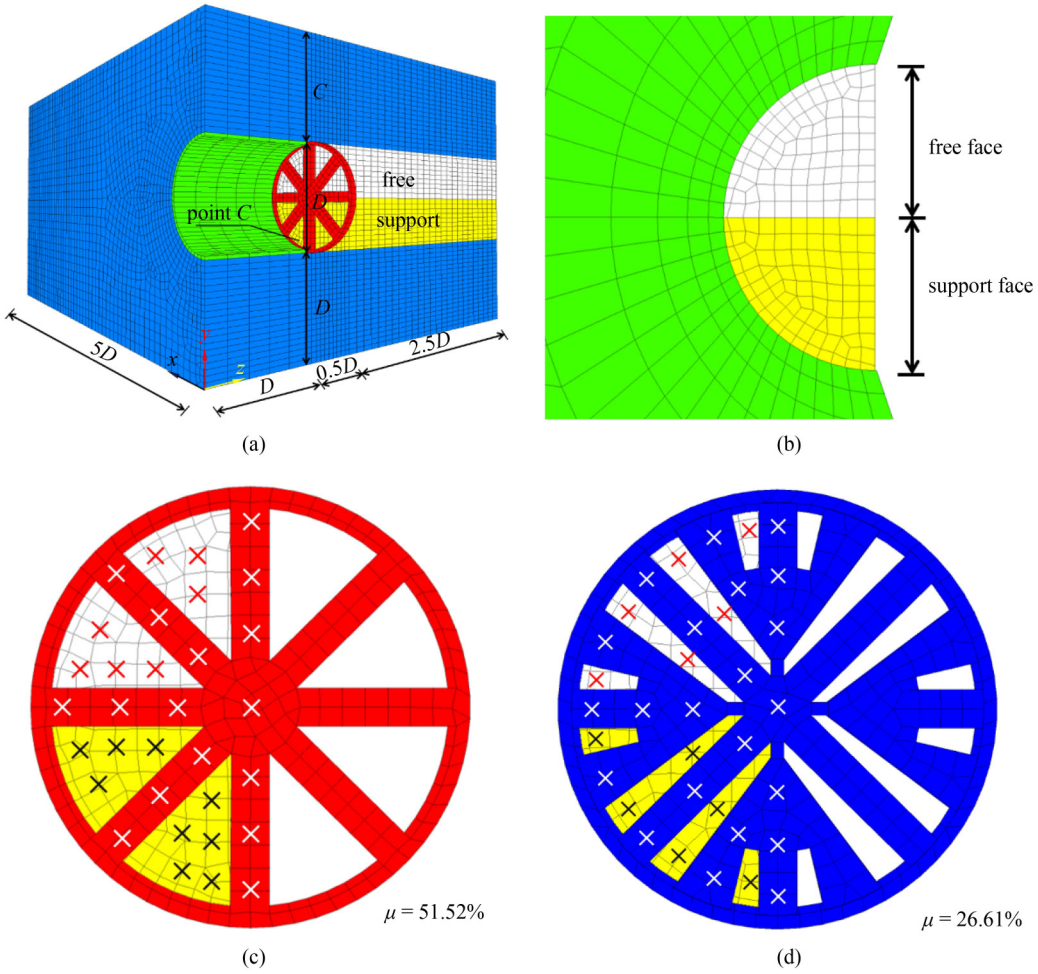

Fig. 5 Schematic diagram of model: (a) integral model; (b) tunnel face; (c) spoke cutterhead; (d) spoke-panel cutterhead. Notes: red cross: uniform support pressure; black cross: uniform support pressure + gradient support pressure; white cross: static earth pressure.

Table 1 Parameters of soil, cutterhead, and segment

material	unit weight (kN·m^3)	cohesion (kPa)	internal friction angle (°)	Poisson's ratio	elastic modulus (MPa)
soil	18.0	7	17	0.30	24
cutterhead	78.5	–	–	0.26	2.06×10^5
shell	28.0	–	–	0.16	2.3×10^4

value. The number of steps N required to return to the equilibrium state of ground stress is determined. For the spoke cutterhead model, the N is 3396, whereas it is approximately 3681 for the spoke-panel cutterhead model. Compared with classical stress control methods [46], this method can improve the calculation accuracy and reduce the calculation time required to reach the plastic flow state, particularly when the desired accuracy for the results is high [47].

To verify the proposed method, the results of numerical simulations obtained from FLAC3D were compared with the results obtained using the proposed method. The gradient coefficient was set to 3.0. Figure 6 shows the limit support pressure σ_S for different support ratios and aperture ratios. Based on comparison, the theoretical results were consistent with the numerical simulations. This indicates that σ_S gradually increased with the empty level of the excavation chamber. The rate of increase of σ_S decreased gradually. For μ = 100%, the average increase rate when $n \geqslant 0.3$ was 79.34%, whereas it was only 2% when $n \leqslant 0.3$. This indicates that tunnel face stability was primarily sustained by the uniformly distributed earth pressure and compressed air pressure under a low support ratio. In addition, σ_S decreased with the aperture ratio. For the spoke-panel cutterhead models ($n \geqslant 0.8$), σ_S reduced to zero. Under this condition, the tunnel face can maintain a steady-state supported only by the cutterhead, and a chamber opening at atmospheric pressure is theoretically feasible.

Next, the variation in the horizontal displacement of the

non-cutterhead area for different support ratios is analyzed. According to Xu et al. [41], the position with the maximum horizontal displacement is at the bottom of the tunnel face. As shown in Fig. 7, the results are consistent with the numerical simulation results of this study. The displacement of the lower opening area is significantly larger than that of the top and cutterhead areas. Consequently, point *C*, which is at the center of the lowest opening area, was selected as the monitoring point, and its specific position is shown in Fig. 5(a). The support pressure applied to the tunnel face is the result yielded by the proposed method. The horizontal displacements of point *C* for the three aperture rate cases are shown in Fig. 7. The displacement changed equally as the support ratio decreased. Each case indicated instability trend lines extending forward from the vault and the bottom of the arch. This indicates that local failure will not occur in the open zones of the tunnel face owing to the decrease in the support ratio. This further confirms the rationality of the proposed method.

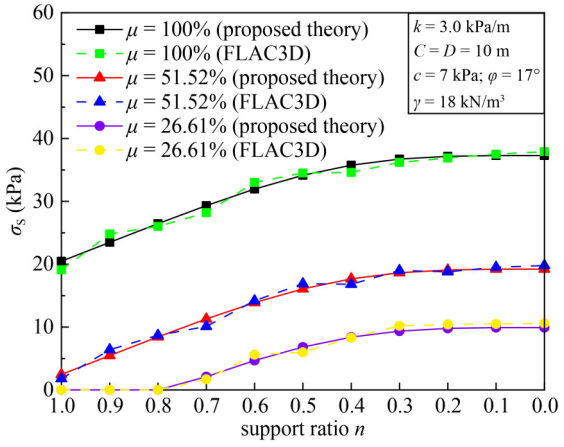

Fig. 6 Limit support pressure vs. support ratio for different aperture ratios.

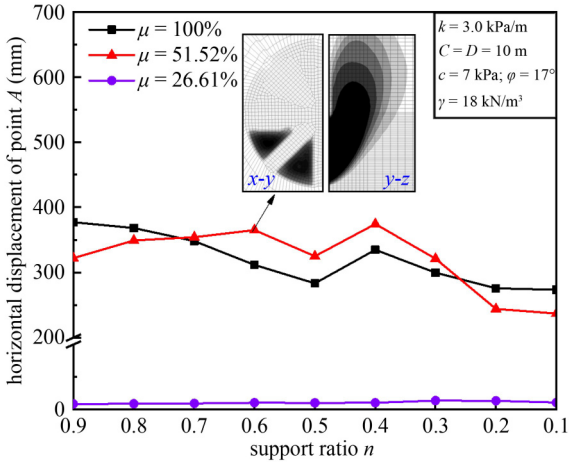

Fig. 7 Horizontal displacement of point *C*.

4 Parametric study

Figure 8 shows the effect of the tunnel diameter *D* and stratum internal frictional angle φ on the critical support pressure σ_S. An increasing demand for transportation has resulted in an increase in the shield tunnel diameter. A few tunnels measured approximately 20 m in diameter; hence, the range of tunnel diameter was set as 5–20 m for the analysis. The cover depth-to-diameter ratio ranged from 0.5 to 2.0, whereas φ ranged from 10° to 30°. The gradient coefficient was set as 3.0 kPa/m. As shown in Fig. 8, the required limit support pressure increased gradually with *D*. This indicates that the pressure difference between the support pressure and external soil pressure increased. Similarly, a larger *D* implies a higher risk of face collapse. In addition, σ_S decreased with φ, indicating that the support pressure required to maintain the stability of the tunnel face is much higher under unsatisfactory geological conditions.

Figure 9 shows the effects of the support pressure gradient *k* and soil cohesion *c* on the limit support pressure. The following analysis is based on *k* and *c* values ranging from 0 to 15 kPa/m and 0 to 15 kPa, respectively. Here, $k = 0$ indicates that the support pressure is uniformly distributed on the entire tunnel face. In this condition, the effect of the supporting medium specific gravity is not considered. The theoretical calculation results based on $k = 0$ can be regarded as results based on a compressed air pressure maintenance chamber opening. The limit support pressure decreased gradually as *k* increased (see Fig. 9). When σ_S decreased to 0, the pressure distribution mode changed to a triangular distribution, which implies that the stability of tunnel face is overestimated by considering a uniformly distributed support pressure. This further indicates that increasing the specific gravity of the support medium to an appropriate level can improve the stability of the

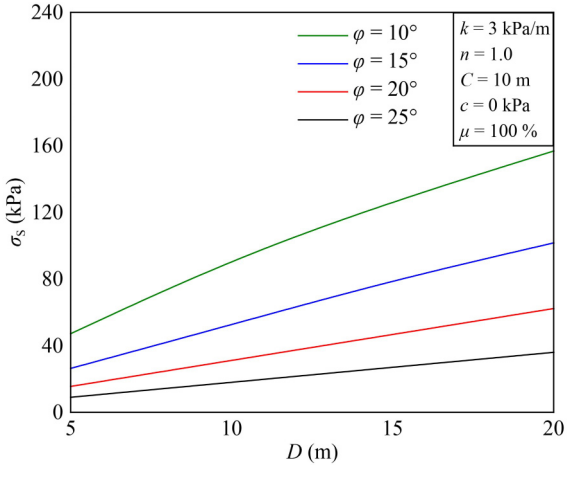

Fig. 8 Effects of tunnel diameter and stratum internal frictional angle on limit support pressure σ_S.

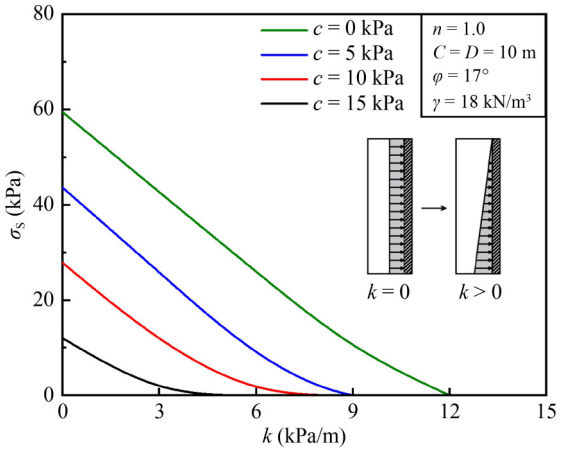

Fig. 9 Effects of support pressure gradient and stratum cohesive on limit support pressure σ_S.

tunnel face. For example, engineers can use additives to improve the density of slurries used for constructing shields [48]. Meanwhile, σ_S decreased as c increased. This indicates that increasing the stratum strength in front of the tunnel face can reduce the risk of collapse when the shield machine is shut down.

5 Discussion

Soil reinforcement at the shield end is an essential component of shield machine maintenance during outages. Selecting a suitable reinforcement method for the end soil is necessary to guarantee engineering safety. Both sandy soil and saturated clay lack adequate self-stability and water repellency. When the tunnel face is exposed after the end seal is removed, soil collapse and water bursts tend to occur at the front soil. Currently, chemical reinforcement is one of the most typically used stratum reinforcement methods. Examples of chemical reinforcement include the liquid grouting, high-pressure rotating spouting, and deep agitation [49]. In these methods, cement grout or silica gel chemical slurries are used to bond grout with soil particles via perfusion pressing, high-pressure spraying, and deep stirring through pneumatic, hydraulic, or electrochemical principles. Consequently, the stratum strength improves macroscopically, i.e., the cohesion of the stratum improves significantly. Meanwhile, the internal friction angle of the mixed material increases indirectly. Based on typical values of internal friction angle for soil–cement systems, the internal friction angle of the reinforced stratum was set to 20°–30° [50].

In this study, the unconfined compressive strength of the stratum when σ_S decreased to 0 is defined as the lower limit value of the critical reinforcement strength q_{ul}. The critical reinforcement range d_S is defined as the distance between the slip surface edge of the failure mechanism and the tunnel face (as shown in Fig. 10). The detailed calculation procedure is as follows. 1) The internal friction angle of the stratum is set as a fixed value and calculated repeatedly until $\sigma_S = 0$ by adjusting the cohesion. 2) The open zone areas for different aperture rate conditions are determined. Based on the principle of area equivalence, the equivalent diameter R' of the opening area is calculated using the formula $n\pi R^2 = nR'^2$. Local failure is assumed to occur in the opening area if $\sigma_S < 0$. 3) The collapse failure mechanism is determined and the limit reinforcement range d_S is measured.

Figure 11 shows the effects of the internal friction angle and aperture rate on q_{ul}. The results show that q_{ul} decreased gradually as φ increased, whereas it increased significantly with μ. This indicates the non-negligible support effect of the cutterhead. For the cases where $\varphi >$ 25°, the decrease rate of q_{ul} almost stabilized. Based on the computation results, local failure occurred at the opening area in all limit conditions when $\varphi = 30°$. Thus, a multiple factor s must be specified for q_{ul}, i.e., the proposed value q_{up} should be equal to sq_{ul}. The cutterhead of the shield tunneling machine cannot easily cut the reinforcement stratum and can be locked if the reinforcement strength is extremely high. After performing several trial calculations in MATLAB, s was set as 1.49. The stability of tunnel face was confirmed by verifying the area equivalence. Figure 12 shows the variation in the limit reinforcement range d_S with φ. As φ increased, the reinforcement strength increased rapidly in the φ range of 20°–25°. The change rate stabilized when $\varphi > 25°$.

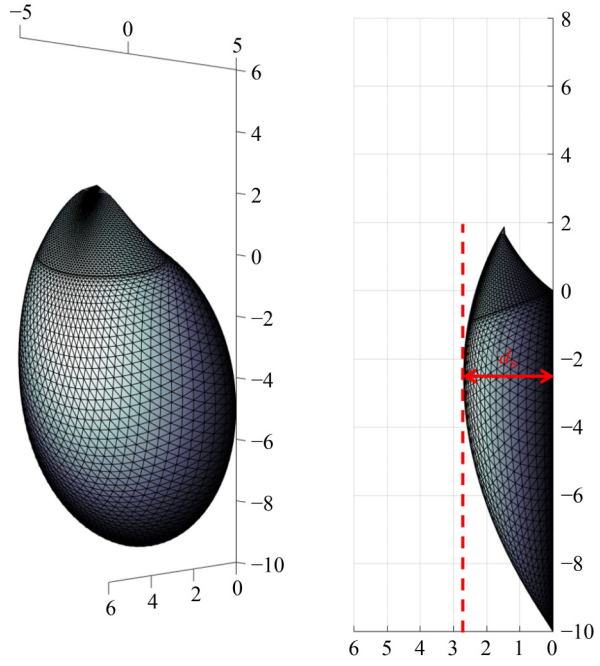

Fig. 10 Schematic diagram of limit reinforcement range d_S.

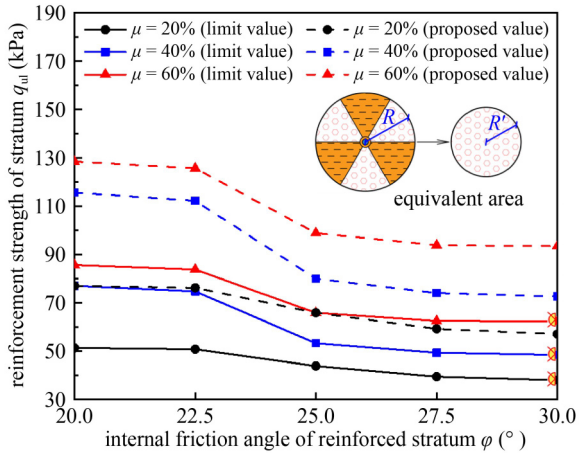

Fig. 11 Effects of internal friction angle and aperture ratio on stratum reinforcement strength q_{ul}.

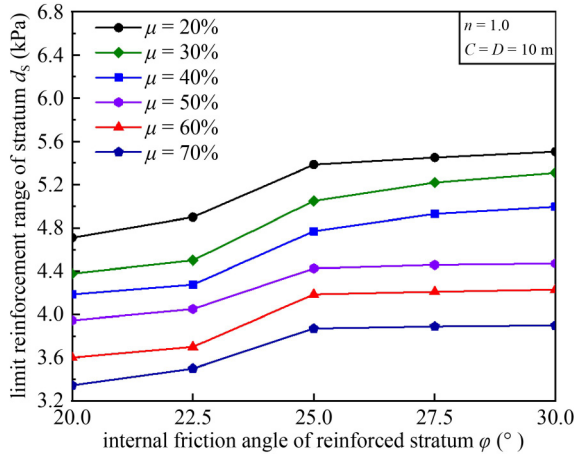

Fig. 12 Effects of internal friction angle and aperture ratio on stratum reinforcement range d_S.

6 Conclusions

Herein, an active failure mechanism for a non-fully supported mode with cutterhead support under a shield machine shutdown period was proposed. The proposed mechanism can be used to determine the limit support pressure with different aperture ratios for maintaining tunnel face stability. The main results are as follows.

1) Assuming a uniformly supported support pressure, the stability of the tunnel face was overestimated. Increasing the specific gravity of the supporting medium to an appropriate level reduced the collapse risk when the support ratio exceeded 0.3. The limit of compressed air pressure increased significantly as the support ratio decreased.

2) The required support pressure increased gradually with D. Unsatisfactory stratum conditions corresponded to higher risks of tunnel face collapse. For the active failure mechanism, the effect of the cutterhead was unfavorable. The support pressure required for maintaining the tunnel face stability was much lower when cutterhead support was implemented.

3) Soil reinforcement at the shield end is typically implemented to guarantee the stability of the tunnel face during shield machine maintenance. The limit reinforcement strength of the stratum increased significantly with the aperture ratio. Conversely, the limit reinforcement range was short when the aperture ratio was high. To avoid local failure on the tunnel face, the reinforcement strength was multiplied based on the limit value, and the multiple factor was set as 1.49. This approach can serve as a basis for soil reinforcement at the shield end.

The model proposed herein cannot consider the seepage field and is suitable only for dry conditions. Hydraulic conditions will adversely affect the limit support pressure. In addition, changes in the cutter can increase the risk of water bursting into the chamber. Further analyses should be conducted in future studies. The addition of a seepage field will be considered in subsequent investigations.

Acknowledgements The authors gratefully acknowledge financial support from the Joint Funds of the National Natural Science Foundation of China (Grant No. U1830208) and the National Natural Science Foundation of China (Grant No. 52008021).

References

1. Hu X, Zhang Z, Kieffer S. A real-life stability model for a large shield-driven tunnel in heterogeneous soft soils. Frontiers of Structural and Civil Engineering, 2012, 6(2): 176−187
2. Geng Z, Jin D, Yuan D. Face stability analysis of cohesion-frictional soils considering the soil arch effect and the instability failure process. Computers and Geotechnics, 2023, 153: 105050
3. Liu X X, Shen S L, Xu Y S, Yin Z Y. Analytical approach for time-dependent groundwater inflow into shield tunnel face in confined aquifer. International Journal for Numerical and Analytical Methods in Geomechanics, 2018, 42(4): 655−673
4. Liu X X, Shen S L, Zhou A, Xu Y S. Evaluation of foam conditioning effect on groundwater inflow at tunnel cutting face. International Journal for Numerical and Analytical Methods in Geomechanics, 2019, 43(2): 463−481
5. Ren D J, Shen S L, Chai J C, Zhou A. Analysis of disc cutter failure in shield tunnelling using 3D circular cutting theory. Engineering Failure Analysis, 2018, 90: 23−35
6. Ren D J, Shen S L, Arulrajah A, Cheng W C. Prediction model of TBM disc cutter wear during tunnelling in heterogeneous ground. Rock Mechanics and Rock Engineering, 2018, 51(11): 3599−3611
7. Elbaz K, Shen S L, Zhou A, Yin Z Y, Lyu H M. Prediction of disc cutter life during shield tunneling with AI via the incorporation of a genetic algorithm into a GMDH-type neural network. Engineering (Beijing), 2021, 7(2): 238−251
8. Lyu H M, Shen S L, Zhou A, Yin Z Y. Assessment of safety status of shield tunnelling using operational parameters with enhanced SPA. Tunnelling and Underground Space Technology, 2022, 123:

104428
9. Zhang X, Tang S, Wu J, Chen P, Tang J, Tu X. Prediction and analysis of abrasiveness of dense sandy stratum by slurry shield at Sutong GIL utility tunnel engineering. Journal of Engineering Geology, 2017, 25(5): 1364−1373
10. Zhang W, Koizumi A. Behavior of composite segment for shield tunnel. Tunnelling and Underground Space Technology, 2010, 25(4): 325−332
11. Tan X, Chen W, Wu G, Wang L, Yang J. A structural health monitoring system for data analysis of segment joint opening in an underwater shield tunnel. Structural Health Monitoring, 2020, 19(4): 1032−1050
12. Wei Z, Fanlu M, Zhanhu Y, Daiwei W, Teng J. Technical status and case study on intervention in the shield chamber. Modern Tunnelling Technology, 2015, 52(1): 9−18 (in Chinese)
13. Rezaei A H, Shirzehhagh M, Golpasand M R B. EPB tunneling in cohesionless soils: A study on Tabriz Metro settlements. Geomechanics and Engineering, 2019, 19(2): 153−165
14. Xue Y, Li X, Qiu D, Ma X, Kong F, Qu C, Zhao Y. Stability evaluation for the excavation face of shield tunnel across the Yangtze River by multi-factor analysis. Geomechanics and Engineering, 2019, 19(3): 283−293
15. Jin D, Zhang Z, Yuan D. Effect of dynamic cutterhead on face stability in EPB shield tunneling. Tunnelling and Underground Space Technology, 2021, 110(1): 103827
16. Wang H, Huang M, Lv X, Zhou W. Upper-bound limit analysis of stability of shield tunnel face considering seepage. Chinese Journal of Geotechnical Engineering, 2013, 35(4): 1696−1704 (in Chinese)
17. Tang X W, Liu W, Albers B, Savidis S. Upper bound analysis of tunnel face stability in layered soils. Acta Geotechnica, 2014, 9(4): 661−671
18. Yang X L, Zhang R. Collapse analysis of shallow tunnel subjected to seepage in layered soils considering joined effects of settlement and dilation. Geomechanics and Engineering, 2017, 13(2): 217−235
19. Zou J, Chen G, Qian Z. Tunnel face stability in cohesion-frictional soils considering the soil arching effect by improved failure models. Computers and Geotechnics, 2019, 106: 1−17
20. Juneja A, Hegde A, Lee F H, Yeo C H. Centrifuge modelling of tunnel face reinforcement using forepoling. Tunnelling and Underground Space Technology, 2010, 25(4): 377−381
21. Liu W, Zhao Y, Shi P, Li J, Gan P. Face stability analysis of shield-driven tunnels shallowly buried in dry sand using 1-g large-scale model tests. Acta Geotechnica, 2018, 13(3): 693−705
22. Liu X Y, Fang H Y, Wang F M, Yuan D J. Horizontal trap-door investigation on face failure zone of shield tunneling in sands. Journal of Central South University, 2021, 28(3): 866−881
23. Lei H, Zhang Y, Hu Y, Liu Y. Model test and discrete element method simulation of shield tunneling face stability in transparent clay. Frontiers of Structural and Civil Engineering, 2021, 15(1): 147−166
24. Paternesi A, Schweiger H F, Scarpelli G. Numerical analyses of stability and deformation behavior of reinforced and unreinforced tunnel faces. Computers and Geotechnics, 2017, 88: 256−266
25. Zhang Z X, Hu X Y, Scott K D. A discrete numerical approach for modeling face stability in slurry shield tunnelling in soft soils. Computers and Geotechnics, 2011, 38(1): 94−104
26. Mollon G, Dias D, Soubra A H. Rotational failure mechanisms for the face stability analysis of tunnels driven by a pressurized shield. International Journal for Numerical and Analytical Methods in Geomechanics, 2011, 35(12): 1363−1388
27. Perazzelli P, Leone T, Anagnostou G. Tunnel face stability under seepage flow conditions. Tunnelling and Underground Space Technology, 2014, 43: 459−469
28. Pan Q, Dias D. The effect of pore water pressure on tunnel face stability. International Journal for Numerical and Analytical Methods in Geomechanics, 2016, 40(15): 2123−2136
29. Ji X, Ni P, Barla M, Zhao W, Mei G. Earth pressure on shield excavation face for pipe jacking considering arching effect. Tunnelling and Underground Space Technology, 2018, 72: 17−27
30. Kirsch A. Experimental investigation of the face stability of shallow tunnels in sand. Acta Geotechnica, 2010, 5(1): 43−62
31. Chen R P, Li J, Kong L G, Tang L J. Experimental study on face instability of shield tunnel in sand. Tunnelling and Underground Space Technology, 2013, 33: 12−21
32. Qarmout M, König D, Gussmann P, Thewes M, Schanz T. Tunnel face stability analysis using Kinematical Element Method. Tunnelling and Underground Space Technology, 2019, 85: 354−367
33. Zhu W B, Ju S J. Shield Tunneling Technology in Mixed Face Ground Conditions. Beijing: China Science and Technology Press, 2006 (in Chinese)
34. Wang H X. Type selection of the head aperture ratio of EPB shield cutter heads and adaptability to stratum characteristics. China Civil Engineering Journal, 2010, 43(3): 88−92 (in Chinese)
35. Min F, Zhu W, Lin C, Guo X. Opening the excavation chamber of the large-diameter size slurry shield: A case study in Nanjing Yangtze River Tunnel in China. Tunnelling and Underground Space Technology, 2015, 46: 18−27
36. Wang J, He C, Wang C, Chen Z Q, Tang R. Face stability analysis of EPB shield tunnel in sand. Chinese Journal of Geotechnical Engineering, 2018, 40(1): 177−185 (in Chinese)
37. Hu X, Cheng J, Ju J W. Influence of the cutterhead configuration and operation parameters on the face stability of EPB shield tunnels in dry granular soils. International Journal of Geomechanics, 2021, 21(5): 04021050
38. Zhu W, Qian Y, Wang L, Hu J, Xing H, Lu K. Problems and measures of earth pressure balance shield during construction with the unfilled chamber. China Journal of Highway and Transport, 2020, 33(12): 224−234 (in Chinese)
39. Zhang Z, Huang M, Zhang C, Jiang K, Bai Q. Analytical prediction of tunneling-induced ground movements and liner deformation in saturated soils considering influences of shield air pressure. Applied Mathematical Modelling, 2020, 78: 749−772
40. Nagel F, Meschke G. An elasto-plastic three phase model for partially saturated soil for the finite element simulation of compressed air support in tunnelling. International Journal for Numerical and Analytical Methods in Geomechanics, 2010, 34(6): 605−625
41. Xu Q, Zhu H, Ding W, Ge X. Laboratory model tests and field investigations of EPB shield machine tunnelling in soft ground in Shanghai. Tunnelling and Underground Space Technology, 2011,

26(1): 1−14
42. Idinger G, Aklik P, Wu W, Borja R I. Centrifuge model test on the face stability of shallow tunnel. Acta Geotechnica, 2011, 6(2): 105−117
43. Qiang Y, Zhao M, Lin J, Cheng L, Li L, He Z. Research on coefficient of earth pressure at rest. Rock and Soil Mechanics, 2013, 34(3): 727−730 (in Chinese)
44. Chen W F. Limit Analysis and Soil Plasticity. Amsterdam: Elsevier, 1975
45. Mollon G, Dias D, Soubra A H. Probabilistic analysis of circular tunnels in homogeneous soil using response surface methodology. Journal of Geotechnical and Geoenvironmental Engineering, 2009, 135(9): 1314−1325
46. Yu L, Zhang D, Fang Q, Cao L, Zhang Y, Xu T. Face stability of shallow tunnelling in sandy soil considering unsupported length. Tunnelling and Underground Space Technology, 2020, 102: 103445
47. Yang W, Zheng J, Zhang R, Qiao Y. Face stability analysis of shield tunnel considering variabilityof soil parameters and support pressure in clay. Journal of Civil and Environmental Engineering, 2021, 43(6): 27−37
48. Min F, Zhu W, Han X. Filter cake formation for slurry shield tunneling in highly permeable sand. Tunnelling and Underground Space Technology, 2013, 38: 423−430
49. Pani L, Stochino F. Punching of reinforced concrete slab without shear reinforcement: Standard models and new proposal. Frontiers of Structural and Civil Engineering, 2020, 14(5): 1196−1214
50. Zhang H, Xing H. Mechanical characteristic and microstructure of salt-rich cement soil. Bulletin of Engineering Geology and the Environment, 2022, 81(3): 1−12